Smart Zeolites: New Forms of Tungsten and Molybdenum Oxides

GEOFFREY A. OZIN,*,† SAIM ÖZKAR,‡ AND RICHARD A. PROKOPOWICZ†

Advanced Zeolite Materials Science Research Group, Lash Miller Chemical Laboratories, The University of Toronto, 80 St. George Street, Toronto, Ontario, Canada M5S 1A1, and Chemistry Department, Middle East Technical University, Ankara, Turkey

In this Account, we describe our recent research efforts involving the use of volatile hexacarbonylmolybdenum and -tungsten compounds, as precursors in the synthesis of highly organized assemblies of molecular dimension molybdenum and tungsten oxides, encapsulated within the diamond network of 13-Å supercages found in zeolite Y.[2-8] These assemblies are extremely uniform in terms of their nuclearity and structure, and their exclusive internal confinement inside of and lack of significant perturbation of the zeolite Y host. In these materials, the bulk form of the metal oxide has essentially been reconstituted within the nanoscale void spaces of a crystalline aluminosilicate framework host. The electronic and structural properties of these molecular metal oxide arrays can be easily manipulated as a result of their facile redox interconvertibility, and the further capability of fine tuning their electronic environment by choosing which charge-balancing cation is present in the supercage.

Bulk forms of WO_3 and MoO_3, which possess octahedral building blocks arranged into open framework, layer, and tunnel structures,[1] are probably most famous for their ability to reversibly accept metal cations and protons into their internal void spaces and electron-charge-transfer equivalents into their conduction bands. This fascinating property enables them to function as "intelligent" materials in, for example, electrochromic windows, mirrors and displays, rechargeable solid-state batteries, pH–microelectrochemical transistors, and

chemical sensors. In addition, their narrow-band-gap semiconductor properties allow them to be usefully exploited in liquid junction solar and electrochemical cells. Finally, the facile and reversible loss of lattice oxygen found in the Magnéli type MO_{3-x} non-stoichiometric crystallographic shear phases endows them with the ability to perform selective hydrocarbon oxidation chemistry and catalysis.[1] In this same regard, the $n[MO_{3-x}]-M'_{56}Y$ materials discovered in the course of our research, being tunable over the entire loading and composition range (M = Mo, W; M' = H, Li, Na, K, Rb, Cs; $0 < n \leq 32$; $0 \leq x \leq 1$), can be considered to be "smart zeolites".

The Tungsten Oxide Systems

Synthesis of Zeolite-Encapsulated Metal Oxides. In the synthesis of various tungsten and molybdenum oxides in zeolite Y, volatile hexacarbonylmetal(0) compounds are sublimed into the zeolite Y host, where they become irreversibly anchored exclusively in the large α-cages. The saturation loading which can be attained is two molecules per α-cage (16 per unit cell). The metal carbonyl is next converted in an O_2 atmosphere to the intrazeolite metal(VI) oxide by photooxidation and may be subsequently thermally reduced in vacuum to yield encapsulated MO_{3-x} moieties (where $0 \leq x \leq 1$). The reduction is reversible by heating in an O_2 atmosphere at 300–400 °C. Following photooxidation, half of the α-cage void volume in the host is freed so that subsequent precursor (saturation level)

Geoffrey A. Ozin was born in London, England, in 1943, completed his undergraduate work in chemistry at King's College, London University, obtained his Ph.D. in inorganic chemistry at Oriel College, Oxford University, in 1967, and was an ICI post doctoral fellow at Southampton University in 1967–1969. He joined the chemistry faculty at the University of Toronto as an assistant professor in 1969, where he is now a full professor. His current research is exclusively in the area of solid-state chemistry with a thrust toward advanced zeolite materials science. The emphasis of his work is on the synthesis and characterization of novel nanoporous materials and their structure–property–function relationships.

Saim Özkar was born in Elazig, Turkey, in 1949, completed his undergraduate study in chemical engineering at the Technical University of Istanbul, Turkey, in 1972, and then worked for two years in industry. He obtained his Ph.D. in inorganic chemistry at the Technical University of Munich in 1976 before joining the Chemistry Department of the Middle East Technical University, Ankara, Turkey, as an assistant professor in 1979, where he is now a full professor. His main research interests involve organometallic photochemistry of the group 6B metal carbonyls and synthesis, characterization, and dynamic NMR studies of novel carbonyl–olefin–metal complexes. His current research concerns the solid-state chemistry of intrazeolite organometallics and metal carbonyls.

Richard A. Prokopowicz was born in Galt (now Cambridge), Ontario, Canada, in 1960. He completed his undergraduate work at the University of Waterloo, where he obtained a B.A.Sc. in chemical engineering in 1983. In 1989 he received a Ph.D. in physical chemistry from the University of Toronto. The subject of his doctoral thesis was the synthesis and characterization of novel materials produced by metal vapor synthesis techniques. He is currently conducting research as a member of the Advanced Zeolite Materials Science Group, Department of Chemistry, at the University of Toronto. His major interests lie in the areas of characterizing novel zeolite–based materials.

* To whom correspondence should be sent.
† The University of Toronto.
‡ Middle East Technical University.
(1) Rao, C. N. R.; Gopalakrishnan, J. *New Directions in Solid State Chemistry*; Cambridge University Press: Cambridge, 1986.
(2) Ozin, G. A.; Prokopowicz, R. A.; Özkar, S. Intrazeolite Nonstoichiometric Tungsten Oxides $n[WO_{3-x}]-Na_{56}Y$; $0 < n \leq 32, 0 \leq x \leq 1$. *J. Am. Chem. Soc.*, in press.
(3) Özkar, S.; Ozin, G. A.; Prokopowicz, R. A. Photooxidation of Hexacarbonylmolybdenum(0) in Sodium Zeolite Y Yields Redox Interconvertible Molybdenum(VI) Oxide and Molybdenum(IV) Oxide Monomers. *Chem. Mater.*, in press.
(4) Ozin, G. A.; Malek, A.; Prokopowicz, R. A.; Macdonald, P. M.; Özkar, S.; Moller, K.; Bein, T. Doping and Band-Gap Engineering of an Intrazeolite Tungsten(VI) Oxide. In *New Directions in Zeolite Chemistry. Mater. Res. Soc. Symp. Proc.* 1991, 233, 109.
(5) Moller, K.; Bein, T.; Özkar, S.; Ozin, G. A. *J. Phys. Chem.* 1991, 95, 5276.
(6) Özkar, S.; Ozin, G. A.; Moller, K.; Bein, T. *J. Am. Chem. Soc.* 1990, 112, 9575.
(7) Ozin, G. A.; Özkar, S. *J. Phys. Chem.* 1990, 94, 7556.
(8) Ozin, G. A.; Özkar, S.; Macdonald, P. M. *J. Phys. Chem.* 1990, 94, 6939.

554 *Acc. Chem. Res., Vol. 25, No. 12, 1992*

Ozin et al.

impregnations/photooxidations (SIP) can be carried out; the stepwise loading proceeds as 16, 24, 28, 30, ..., 32 per unit cell.

Structural Characterization: Stoichiometries and Anchoring. Many structural details of the various intrazeolite tungsten and molybdenum oxide materials, as well as details of their framework-anchoring interactions, have been elucidated through the use of such techniques as EXAFS, FTIR, ^{29}Si MAS-NMR, and ^{27}Al/^{23}Na DOR-NMR spectroscopies, HR-TEM, and gravimetry. These have demonstrated that each of the impregnation, photooxidation, and thermal treatment steps is clean and quantitative. Every sample exhibits a homogeneous appearance. The techniques[2] of quantitative PXRD, STEM-EDX, ^{29}Si/^{27}Al MAS-NMR, and XPS have been applied to examine all of the materials from the precursor stage through each of the photooxidations, reductive eliminations of O_2, and subsequent reoxidation in O_2. These demonstrate that, during all such reactions, the crystal morphology and degree of crystallinity of the $M'_{56}Y$ host remain unaltered, and the integrity of the framework stays intact, with the unit cell dimension of the cubic $M'_{56}Y$ host remaining essentially unaltered at $a_0 = 24.690$–24.694 Å. Furthermore, there was no evidence for the formation of bulk WO_{3-x} oxides, nor for the deposition of surface carbon (at the 1000 ppm detection sensitivity of XPS). The surface W:Na:Al elemental ratios were always close to, but slightly less than, the bulk elemental analysis. No superlattice reflections were observed, nor evidence for segregation into domains.

Adsorption-induced ^{23}Na MAS/DOR-NMR chemical shifts, FAR-IR Na^+ translatory mode frequency shifts, and MID-IR $\nu(OH_\alpha)$ hydrogen-bonding shifts[2,8] provide indirect and complementary evidence for the selective anchoring of WO_{3-x} moieties to α-cage M^+ cations in $n[WO_{3-x}]$–$Na_{56-m}H_mY$, for example (where $m = 8, 16$). These experiments provide additional support for the homogeneity of the distribution of entrapped WO_{3-x} guests and moreover enable one to monitor the birth and population growth of these moieties over the entire loading range ($n = 0$–32). In particular, it appears that in the special case of half-loading ($n = 16$) and full-loading ($n = 32$), ordered supralattices containing $2(WO_{3-x})$ and $4(WO_{3-x})$ guests per α-cage, respectively, have been created.

Taken together, the above observations point to a sequence of events in which all WO_{3-x} moieties remain internally confined and homogeneously dispersed throughout the internal void structure of the zeolite Y host. Additional support for the above proposals stems from high-resolution electron microscopy. A representative lattice image is shown in Figure 1 for the sample $12[WO_3]$–$Na_{56}Y$. This shows no evidence for the formation of zones of high and low tungsten concentration, either within the zeolite or as bulk WO_3 deposited outside the host.

In the case of the vacuum thermal treatment of $n[WO_3]$–$Na_{56}Y$ (whose behavior typifies that of the other cation frameworks), the evolution of O_2 begins around 200 °C to yield royal blue colored ($0 < n \leq 8$) or metallic blue-gray colored ($8 \leq n \leq 32$) materials having W:O = 1:2.5 at 300 °C. Between 300 and 400 °C, O_2 evolution continues, eventually yielding white ($0 < n \leq 8$) or grayish off-white ($8 \leq n \leq 32$) materials

Figure 1. High-resolution transmission electron micrograph of the sample $12[WO_3]$–$Na_{56}Y$.

having W:O = 1:2. Quantitative reversal of this process can be achieved at 300 °C in O_2, leading to the original material $n[WO_3]$–$Na_{56}Y$, but apparently bypassing the intermediate phase $n[WO_{2.5}]$–$Na_{56}Y$. This sequence of reactions is summarized by

$$n[WO_3]\text{–}M'_{56}Y \xrightarrow[\text{vacuum}]{300\ °C} n[WO_{2.5}]\text{–}M'_{56}Y \xrightarrow[\text{vacuum}]{400\ °C} n[WO_2]\text{–}M'_{56}Y$$
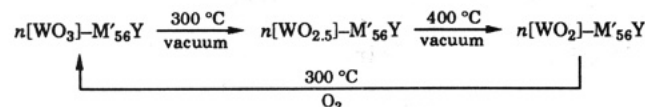$$\xleftarrow[\qquad O_2 \qquad]{300\ °C}$$

Table I presents the results of EXAFS analysis of all samples examined. A qualitative comparison of the k^1-weighted Fourier transforms of the EXAFS $\chi(k)$ functions for all three samples $n[WO_3]$–$Na_{56}Y$ for $n = 16, 28,$ and 32 showed them to be remarkably similar. Results indicate that they possess two short terminal W=O bonds and two long bridging W–O bonds. The k^3-weighted (to emphasize W–W contributions) datasets yielded, again with similarity among all three samples, a short distance to a second tungsten. This bond length and coordination number information for $n = 16, 28,$ and 32 samples is best interpreted in terms of the formation of a *single kind* of tungsten(VI) oxide dimer moiety, namely, W_2O_6, with one per α-cage for $n = 16$, two per α-cage for $n = 32$, and some combination of these two extremes (half- and full-filling) for the intermediate loading $n = 28$. The terminal dioxotungsten bond lengths of 1.75–1.78 Å found in these dimers fall within a range between those normally observed[9,10] for compounds having

(9) Day, V. W.; Klemperer, W. G. *Science* **1985**, *228*, 533.

**Table I. Structural Parameters of the
Zeolite-Encapsulated Tungsten and Molybdenum Oxide
Materials Determined by Analysis of W L_{III}-Edge and
Mo K-Edge EXAFS Data**

sample	atom pair	bond no.	bond distance (Å)	static disorder (Å²)	inner potential (eV)
$16[WO_3]-Na_{56}Y$	W–O	2.2	1.77	0.0008	3.8
	W–O	1.8	1.94	−0.0009	3.8
	W–W	1.3	3.30	0.0019	−6.9
$28[WO_3]-Na_{56}Y$	W–O	2.2	1.75	0.0030	3.6
	W–O	2.2	1.95	0.0010	−3.9
	W–W	1.4	3.24	0.0047	−3.5
$32[WO_3]-Na_{56}Y$	W–O	1.7	1.78	−0.0004	4.1
	W–O	1.9	1.96	0.0008	2.4
	W–W	1.4	3.31	0.0009	−10.0
$16[WO_{2.5}]-Na_{56}Y$	W–O	2.1	1.77	0.0009	6.1
	W–O	1.1	1.94	−0.0011	2.8
	W–W	1.3	3.30	0.0028	−10.0
$32[WO_{2.5}]-Na_{56}Y$	W–O	2.2	1.83	0.0048	5.0
	W–O	0.8	2.00	−0.0034	−4.3
	W–W	3.0	3.30	0.0036	−5.5
$16[WO_2]-Na_{56}Y$	W–O	4.1	1.81	0.0028	0.4
$28[WO_2]-Na_{56}Y$	W–O	4.1	1.79	0.0024	0.8
$32[WO_2]-Na_{56}Y$	W–O	4.0	1.84	0.0040	1.9
$16[WO_3]-Rb_{56}Y$	W–O	0.9	1.80	−0.0009	12.0
	W–O	3.6	2.06	0.0045	−0.6
$16[WO_{2.5}]-Rb_{56}Y$	W–O	0.8	1.76	−0.0008	12.0
	W–O	1.9	1.94	0.0099	0.7
	W–W	1.3	3.31	0.0019	−12.0
$16[WO_2]-Rb_{56}Y$	W–O	3.6	1.83	0.0059	3.2
$16[MoO_3]-Na_{56}Y$	Mo–O	3.2	1.73	0.0000	1.5
	Mo–O	2.8	1.88	0.0019	1.6
$16[MoO_2]-Na_{56}Y$	Mo–O	5.1	1.80	0.0024	0.6

tungsten–oxygen formal bond orders of 2 (e.g., 1.69–
1.70 Å in $[W_6O_{19}]^{2-}$) and 1.5 (e.g., 1.82 Å in $[WO_4]^{2-}$).
This indirectly implies the existence of anchoring
interactions between the terminal dioxotungsten groups
of the W_2O_6 guest and extraframework α-cage Na^+
cations of the $Na_{56}Y$ host. This is in agreement with
spectroscopic measurements described in the other
sections of this work. The tungsten–oxygen bond length
of 1.94–1.96 Å found for the bridging $W(\mu$-$O)_2W$ unit
of the dimer falls in the range expected for doubly
oxygen bridged W^{6+} species (e.g., 1.92 Å found[9] in
$[W_6O_{19}]^{2-}$). Figure 2 contains a representation of the
dimer structural unit (and also the related structural
units found in the various reduction products) which
is fully consistent with the structural data derived from
EXAFS. At loading levels wherein there is more than
one such unit per α-cage, results show that an accu-
mulation of α-cage *dimers of dimers* W_2O_6 takes place,
rather than trimers W_3O_9 and/or tetramers W_4O_{12}.
There are literature examples[11–13] of complexes which
actually contain "pieces" of the dimeric W_2O_6 species
found in $n[WO_3]-Na_{56}Y$.

Qualitative examination of the k^1- and k^3-weighted,
background-removed, Fourier-transformed EXAFS of
the first-stage vacuum reduction products $16[WO_{2.5}]-$
$Na_{56}Y$ and $32[WO_{2.5}]-Na_{56}Y$ showed them to be similar
in terms of W–O and W–W peak positions, but rather
distinct in terms of peak amplitudes. It was determined
that the $16[WO_{2.5}]-Na_{56}Y$ sample had two short ter-

(10) Okada, K.; Morikawa, H.; Marumo, F.; Iwai, S. *Acta Crystallogr.*
1974, *B30*, 1872. Magnéli, A. *Acta Crystallogr.* 1956, *9*, 1038.
(11) Cotton, F. A.; Wilkinson, G. *Advanced Inorganic Chemistry*, 5th
ed.; John Wiley & Sons: New York, 1988.
(12) Ikari, S.; Sasaki, Y.; Ito, T. *Inorg. Chem.* 1989, *28*, 447. Ikari, S.;
Sasaki, Y.; Nagasawa, A.; Kabuto, C.; Ito, T. *Inorg. Chem.* 1989, *28*, 1248.
(13) Rau, M. S.; Kretz, C. M.; Mercando, L. A.; Geoffroy, G. L. *J. Am.
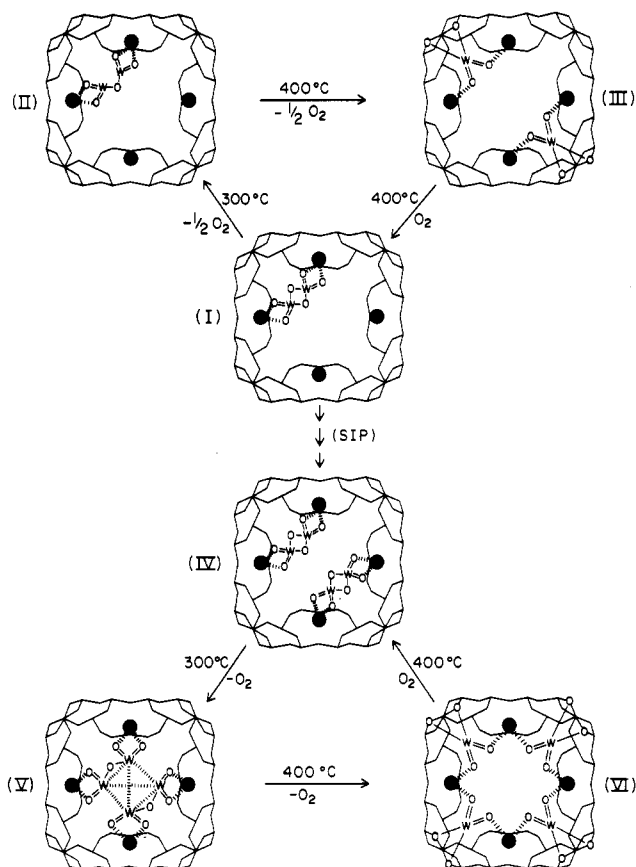Chem. Soc.* 1991, *113*, 7421.

Figure 2. Structures of the various zeolite-encapsulated tungsten
oxides and their thermal vacuum reduction products.

minal W–O bonds but only one long bridging W–O bond
together with a short distance to a second tungsten.
The bond lengths are remarkably similar to those which
were determined for the $16[WO_3]-Na_{56}Y$ sample.
These results, in conjunction with the XPS data
(presented later), are consistent with the presence of
a *single kind* of tungsten(V) oxide dimer moiety W_2O_5
and are also depicted in Figure 2.

Comparison of the structural details of $32[WO_{2.5}]-$
$Na_{56}Y$ and $16[WO_{2.5}]-Na_{56}Y$ show that both of the W–O
bond lengths are increased in the former relative to the
latter (by about 0.06 Å), although they are remarkably
similar with respect to W–W distances ($R_{WW} = 3.30$ Å).
Most significantly, however, the $32[WO_{2.5}]-Na_{56}Y$ sam-
ple has a W–W coordination number of 3, whereas the
coordination number in the case of $16[WO_{2.5}]-Na_{56}Y$
was essentially 1. These data taken together with the
XPS and ^{23}Na MAS/DOR-NMR data presented later
are consistent with the presence of a *single kind* of
α-cage Na^+ cation anchored tungsten(V) oxide tetramer
moiety W_4O_{10} (V in Figure 2).

A summary of the structural details of the 400 °C
reduction products $n[WO_2]-Na_{56}Y$ is included in Figure
2. This second reduction product is strikingly different
from the two aforementioned cases. In particular, the
EXAFS data for the $n[WO_2]-Na_{56}Y$ series indicated a
first shell containing only one W–O distance, and no
evidence of any W–W scattering contribution. That
there is no evidence of W–W backscatter pairs implies
that the distances between the tungsten centers in WO_2
must be much greater than in the aforementioned W_2O_6,
W_2O_5 dimer, and W_4O_{10} tetramer species. Inspection
of the W–O bond lengths and coordination numbers

shows that the $n[WO_2]$–$Na_{56}Y$ samples contain a four-coordinate tungsten oxide moiety having R_{WO} = 1.81–1.84 Å and N_O = 4.0–4.1, which are very similar to the corresponding values for the Na_2WO_4 reference compound. This information (together with the XPS and ^{23}Na MAS/DOR-NMR data presented later) indicates the presence of a *single kind* of tungsten(IV) oxide WO_2 monomer which, unlike the other moieties, is anchored via its tungsten center to two oxygens of a framework four-ring coordination site.

Structural data for the half-loaded $16[WO_{3-x}]$–$Rb_{56}Y$ samples are also listed in Table I. The vacuum-reduced sample $16[WO_{2.5}]$–$Rb_{56}Y$ was determined to be dimeric, and the further reduced $16[WO_2]$–$Rb_{56}Y$ sample was determined to be monomeric, as were their corresponding $Na_{56}Y$ analogues. The $16[WO_3]$–$Rb_{56}Y$ sample, however, was observed to be monomeric and oxygen framework anchored rather than dimeric and cation anchored (as expected from the sodium zeolite system). This was rationalized on the basis of steric limitations posed by the existence of six larger Rb^+, rather than four smaller Na^+ cations in the α-cages. It is thought that $16[WO_{2.5}]$–$Rb_{56}Y$ is able to form a dimeric structure as a result of the flexibility of its single W–O–W bridging bond. A structural difference does seem to exist, however, between the Na^+- and Rb^+-anchored moieties. In the former case, the Na^+ cations and the two W atoms are essentially collinear, with one long and two short W–O distances. In the latter case, the W–O distances are best described as one short and two long. This result is rationalized in terms of a slightly different model, in which the Rb^+ and W centers are not collinear; the two W atoms are likely crowded by the larger Rb^+ cations, so that they protrude more into the center of the α-cage. This distorted (relative to its Na^+ counterpart) dimer structure could possibly result because of the interaction of one of the terminal oxygens with a Rb^+ cation. Evidence also exists for a similar interaction involving the Rb^+ cations, in the case of $16[WO_3]$–$Rb_{56}Y$. Here, an appropriate model is like that of the *fac*-MoO_3 moiety (in $Na_{56}Y$, discussed later), however, distorted in such a way that, instead of three short terminal W=O bonds, two of these are lengthened through their interactions with the Rb^+ cations. Hence the model consists of a single short W=O bond at 1.80 Å and four long W–O distances at 2.06 Å (two bonds and two framework oxygen distances).

DOR-NMR spectroscopy of solids containing quadrupolar nuclei annihilates most of the second-order line-shift and broadening contributions which are not averaged out in the corresponding MAS-NMR experiment.[14] Under these circumstances and using two magnetic field strengths, one is able to obtain high-resolution NMR spectra of, for example, individual Na^+ sites in a $Na_{56}Y$ lattice. One can thus determine how the isotropic chemical shifts, quadrupole coupling constants, intensities, and relaxation times are affected by the presence of an adsorbed guest. Here the Na^+ chemical shifts and line shapes are expected to be sensitive to site-specific oxygen-framework- and cation-anchoring energetics and dynamics. Specific details pertinent to the present materials are published elsewhere.[15]

Figure 3. ^{23}Na solid-state DOR-NMR data for (a) dehydrated $Na_{56}Y$; (b) $16[W(CO)_6]$–$Na_{56}Y$; (c) $16[WO_3]$–$Na_{56}Y$; (d) 16-$[WO_{2.5}]$–$Na_{56}Y$; and (e) $16[WO_2]$–$Na_{56}Y$. The asterisks indicate spinning side bands.

^{23}Na MAS-NMR spectra of $Na_{56}Y$, $n[W(CO)_6]$–$Na_{56}Y$, and the various $n[WO_{3-x}]$–$Na_{56}Y$ samples were all observed to be convolutions of poorly resolved quadrupolar broadened resonances from the various Na^+ sites.[8] The ^{23}Na DOR-NMR results depicted in Figure 3, however, provide a sensitive and direct probe of the $ZONa^+\cdots O$ anchoring interactions in the α-cages. Thus, they more completely define the structure and properties of $W(CO)_6$ and WO_{3-x} guests in zeolite Y.[15] An examination of the DOR-NMR spectra of $n[W$-$(CO)_6]$–$Na_{56}Y$ in a loading dependent study (n = 0, 4, 8, 16) demonstrated a substantial enhancement of the ^{23}Na resonance located around –23 ppm, with increasing values of n. This peak was therefore attributed to the *selective* anchoring of these $W(CO)_6$ guest species to site II Na^+ cations in the α-cages, an assignment which was independently confirmed by a ^{23}Na DOR-NMR study[15] of Tl^+ cation exchange in sodium zeolite Y. The intensities of the resonances at –5 and –41 ppm (assigned to the site I and site I' cations, respectively) were essentially not altered by adsorption of $W(CO)_6$. Upon photooxidation of the parent $16[W(CO)_6]$–$Na_{56}Y$ to the oxide $16[WO_3]$–$Na_{56}Y$, a significant decrease in the intensity of the site II ^{23}Na resonance was observed (Figure 3c). This was rationalized on the basis that twice as many Na^+ cations are involved in the anchoring

(14) Samoson, A.; Lippmaa, E.; Pines, A. *Mol. Phys.* **1988**, *65*, 1013. Chmelka, B. F.; Mueller, K. T.; Pines, A.; Stebbins, J.; Wu, Y.; Zwanziger, J. W. *Nature* **1989**, *339*, 42.
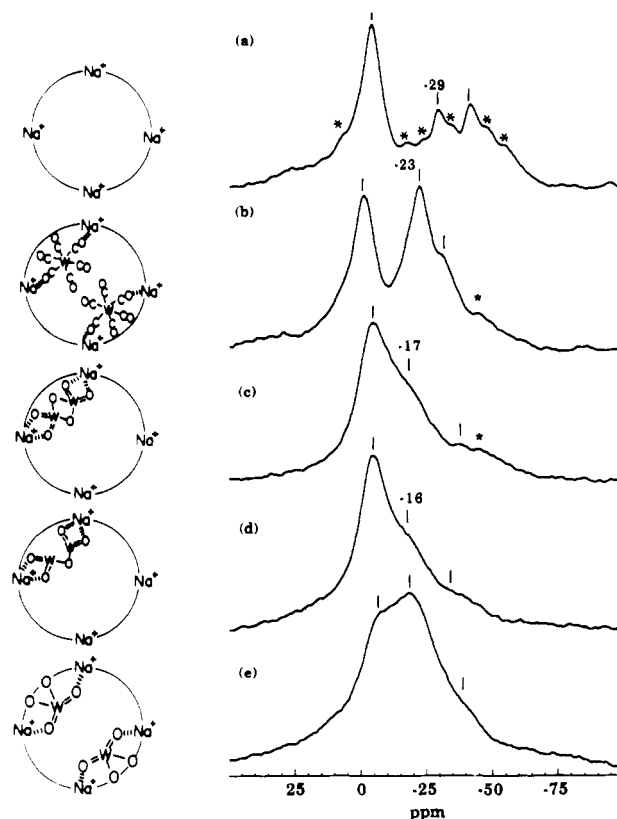
(15) Ozin, G. A.; Özkar, S.; Jelinek, R. Intrazeolite Topotaxy: ^{23}Na DOR-NMR Study of Transition Metal Hexacarbonyls and Oxides Encapsulated in Sodium Zeolite Y. *J. Phys. Chem.* **1992**, *96*, 5949; Extraframework Sodium Cation Sites in Sodium Zeolite Y Probed by ^{23}Na DOR-NMR. *J. Am. Chem. Soc.* **1992**, *114*, 4907. Ozin, G. A.; Özkar, S.; Jelinek, R.; Pastore, H. O. Guest–Host Interactions in Sodium Zeolite Y: A Structural and Dynamical ^{23}Na Double Rotation NMR Study of H_2O, PMe_3, $Mo(CO)_6$, and *cis*-$Mo(CO)_4(PMe_3)_2$ Adsorption in $Na_{56}Y$. *J. Am. Chem. Soc.*, in press.

Smart Zeolites

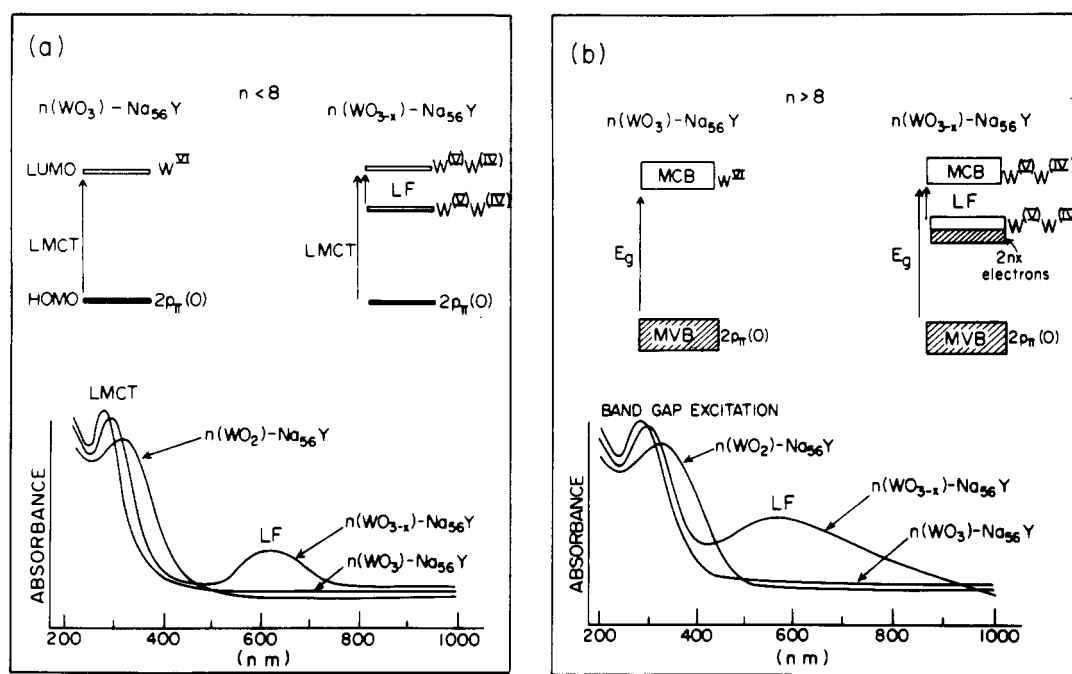*Acc. Chem. Res., Vol. 25, No. 12, 1992* **557**

Figure 4. A comparison of UV–visible reflectance spectra and corresponding qualitative band diagrams for $n[WO_{3-x}]$–$Na_{56}Y$ materials for $x = 0$, $x = 0.5$, and $x = 1$: (a) electronically "uncoupled" samples $(n < 8)$; (b) "coupled" samples $(n \geq 8)$.

of $16[W(CO)_6]$–$Na_{56}Y$ as compared with that of 16-$[WO_3]$–$Na_{56}Y$ (Figure 2). The signal due to the site II ^{23}Na resonance (Figure 3c) in $16[WO_3]$–$Na_{56}Y$ appears as a shoulder at about -15 ppm, on the prominent downfield resonance. The strong downfield shift from the original position (-29 ppm, Figure 3a) is probably a result of the structural differences between $W(CO)_6$ and the W_2O_6 dimer as the α-cage guest. Transformation of the former to the latter is postulated to alter significantly the environment and interaction strength of the anchoring site II Na^+ cations. The spectra shown in Figure 3d,e are also consistent with the structures of the $16[WO_{2.5}]$–$Na_{56}Y$ and $16[WO_2]$–$Na_{56}Y$ materials, as presented in Figure 2. There was virtually no difference between the ^{23}Na DOR-NMR spectra of the W_2O_6 and W_2O_5 loaded samples, as was expected since both are proposed to have the basic *dimer* structure anchored to site II Na^+ cations. In the case of the 16-$[WO_2]$–$Na_{56}Y$ material, however, wherein the structure is proposed to be monomeric and oxygen framework anchored (with the oxygen end of each oxotungsten bond interacting with a site II Na^+ anchoring cation), the NMR spectrum was substantially different from those of the two dimeric samples. In the $16[WO_2]$–$Na_{56}Y$ case, the spectrum features a prominent resonance at -23 ppm, which is attributed to this site II Na^+ anchoring. The ability to collect high-quality *normal* ^{23}Na MAS- and DOR-NMR spectra for all of these systems supports the proposal that these WO_{3-x} moieties are diamagnetic, with spin-paired electronic ground states (this is further reinforced by the UV–vis spectroscopy, which is discussed in the next section).

Electronic and Optical Properties. The techniques of XPS, UV–vis, and EPR spectroscopies have been used in order to gain insight into subtle details of the electronic properties of these materials. In addition to the structural changes afforded by the reductive elimination and oxidative addition of dioxygen to/from the photooxidation products in the $n[WO_{3-x}]$–$Na_{56}Y$ materials, it is possible thereby to manipulate the degree

of n-doping and extent of miniband filling[17] of an intrazeolite tungsten(VI) oxide supralattice. It may be recalled that bulk WO_3 has a distorted ReO_3 structure and is an allowed, indirect band gap semiconductor[16] ($E_g = 2.7$ eV), having an impressive range of solid-state applications[1] including selective hydrocarbon oxidation catalysis.

XPS measurements of the $W(4f_{7/2})$ binding energies (uncertainty of ± 0.4 eV) in $16[WO_{3-x}]$–$Na_{56}Y$ samples were made for $x = 0$, $^1/_2$ and 1. The value of 36.2 eV for $16[WO_3]$–$Na_{56}Y$ is clearly characteristic of W^{6+} having an upward energy shift of roughly 5.9 eV compared to the W^0 precursor $16[W(CO)_6]$–$Na_{56}Y$. It is consistent both with the stoichiometry of WO_3 which was assigned on the basis of gravimetric analyses and with the EXAFS structural results. Likewise, the $W(4f_{7/2})$ binding energy of 34.1 eV measured for the $16[WO_2]$–$Na_{56}Y$ sample is clearly indicative of W^{4+} (in agreement with the stoichiometry WO_2). In the case of the intermediate oxide $16[WO_{2.5}]$–$Na_{56}Y$, the measured core level ionization energy of $W(4f_{7/2}) = 35.6$ eV has been attributed[2] to the existence of a W^{5+}/W^{5+} rather than a mixed-valence W^{4+}/W^{6+} dimer species.

Further details of the structure-related electronic properties of the $n[WO_{3-x}]$–$Na_{56}Y$ materials can be obtained from their optical reflectance spectra. Representative UV–visible spectra are shown in Figure 4. An intense broad blue visible band and a red-shifted UV band are observed on passing from $n[WO_3]$–$Na_{56}Y$ to $n[WO_{2.5}]$–$Na_{56}Y$. This blue band broadens and the UV band red shifts on passing from isolated $(n < 8)$ to coupled $(8 \leq n \leq 32)$ $n[WO_{2.5}]$–$Na_{56}Y$ materials. The blue band disappears and the UV band shifts even further red on passing from $n[WO_{2.5}]$–$Na_{56}Y$ to

(16) Nanthakumar, A.; Armstrong, N. R. In *Semiconductor Electrodes*; Finklea, H. O., Ed.; Elsevier Publ. Co.: Amsterdam, 1988.
(17) Jaros, M. *Physics and Applications of Semiconductor Microstructures*; Oxford University Press: Oxford, 1989.

558 *Acc. Chem. Res., Vol. 25, No. 12, 1992*

Ozin et al.

$n[WO_2]-Na_{56}Y$. The same UV band also experiences a red shift on passing from isolated ($n < 8$) to coupled ($8 \leq n \leq 32$) $n[WO_2]-Na_{56}Y$ materials. This UV absorption in $n[WO_3]-Na_{56}Y$ has been assigned[2] to an interstate $O^{2-}(2p\pi) \rightarrow W^{6+}(5d\pi)$ LMCT excitation for the isolated W_2O_6 dimers ($n < 8$). In the situation of coupled W_2O_6 dimers ($8 \leq n \leq 32$), the loading dependent red shifts of the UV absorption suggest that it may be more appropriate to assign this absorption in terms of an interminiband (MVB → MCB) transition. In the case of the $n[WO_{2.5}]-Na_{56}Y$ ($n < 8$) material, comparison with the $n[WO_3]-Na_{56}Y$ spectrum allowed assignment of the UV band to a $O^{2-}(2p\pi) \rightarrow W^{5+}(5d\pi)$ LMCT transition. This band demonstrated an analogous loading dependent red shift when coupled moieties ($8 \leq n \leq 32$) were compared with the uncoupled ones ($n < 8$). The intense blue visible band was therefore assigned[2] as a $W^{5+} \rightarrow W^{5+}$ (ligand-field, noncentrosymmetric W_2O_5 dimer, dipole and spin allowed) transition, rather than a less likely $W^{4+} \rightarrow W^{6+}$ intervalence-charge-transfer (IVCT) transition. The visible LF band was not observed in the monomeric $n[WO_2]-Na_{56}Y$ ($n < 8$) sample. Furthermore, the $O^{2-}(2p\pi) \rightarrow W^{4+}(5d\pi)$ LMCT band was red shifted (relative to $n[WO_{2.5}]-Na_{56}Y$) and also demonstrated loading dependent shifting and broadening effects as had been observed with the other two oxides. In the case of the spin-paired Na^+-anchored W_2O_5 dimer moiety, it is not unreasonable to expect[2] a $W^{5+} \rightarrow W^{5+}$ LF excitation in the visible region, whereas in the case of a spin-paired oxygen-framework-anchored WO_2 monomer, the corresponding $W^{4+} \rightarrow W^{4+}$ LF excitation would most likely shift into the UV region, where it could be obscured by the intense UV LMCT band.

All of the $n[WO_{3-x}]-Na_{56}Y$ samples were observed to be EPR silent (in the temperature range 300–120 K) yet to yield high-quality ^{23}Na DOR/MAS-NMR spectra. This implies that the entire series is diamagnetic with spin-paired singlet electronic ground states for the W^{4+}-, W^{5+}-, and W^{6+}-containing materials. The same EPR silence and NMR activity[2,15] observed for the tetramer present in every α-cage of $32[WO_{2.5}]-Na_{56}Y$ is attributable to a structure containing two diamagnetic spin-paired singlet electronic ground state $(ZONa)\cdots O_2W^{5+}$-$(\mu-O)W^{5+}O_2\cdots(NaOZ)$ d^1-d^1 dimer units. These are probably "intramolecularly" superexchange coupled across their individual μ-oxo bridge bond and possibly "intermolecularly" exchange coupled across the d^1-d^1 dimer units.

Molybdenum Oxide Systems

Structural Characterization: Stoichiometries and Anchoring.

As with the tungsten systems, vapor-phase impregnation of $Mo(CO)_6$ into vacuum thermally dehydrated $M'_{56}Y$ yields α-cage-encapsulated $n[Mo(CO)_6]-M'_{56}Y$. Furthermore, similar analyses[3] using PXRD, STEM-EDX, $^{29}Si/^{27}Al$ MAS-NMR, and XPS have demonstrated that, for the molybdenum precursor and all subsequent oxide products, the crystal integrity, morphology, and degree of crystallinity of the $M'_{56}Y$ host remain unaltered, as does its unit cell dimension. There was again no evidence for the formation of bulk, externally confined MoO_{3-x} oxides, nor for the deposition of surface carbon (at the 1000 ppm detection sensitivity of XPS).

The single T_{1u} IR active ν_{CO} stretching mode (1984.4 cm^{-1}, in n-hexane) of regular O_h symmetry $Mo(CO)_6$ is split into six resolved bands[6] in $n[Mo(CO)_6]-Na_{56}Y$. The frequency and intensity pattern of this ν_{CO} sextet provides compelling evidence for a C_{2v} or lower symmetry *trans*-$(ZONa)\cdots(OC)Mo(CO)_4(CO)\cdots(NaOZ)$ anchoring geometry for the host-guest complex. Site selective, adsorption-induced FAR-IR cation translatory mode frequency shifts, together with ^{23}Na MAS- and DOR-NMR chemical shifts and intensity alterations,[3,15] further reinforce the proposed anchoring characteristics. The results are essentially identical to those found for anchoring of the tungsten analogs, in which α-cage oxygen six-ring site II Na^+ cations and the oxygen end of two *trans*-carbonyl ligands of the $M(CO)_6$ guest are involved.

A combination of quantitative in situ MID-IR spectroscopy and gravimetry[3] has shown that the photo-induced oxidation of $n[Mo(CO)_6]-Na_{56}Y$, at room temperature in 600 Torr of O_2, cleanly yields $n[MoO_3]-Na_{56}Y$ as a sole product (along with six removable "intrazeolite" CO_2 molecules per $Mo(CO)_6$ guest originally impregnated into the host). Treatment of this white material at 400 °C under vacuum results in the elimination of oxygen, to yield the "puce" colored material whose stoichiometry is $n[MoO_2]-Na_{56}Y$ (over the entire loading range $0 < n \leq 16$). This reduction process can be quantitatively reversed in the presence of O_2 at 400 °C, according to the reaction stoichiometry

$$n[MoO_3]-M'_{56}Y \underset{400\,°C/O_2}{\overset{400\,°C}{\rightleftarrows}} n[MoO_2]-M'_{56}Y$$
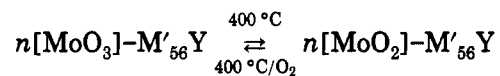
In contrast to results from the tungsten oxide materials, there was no evidence[2] for any intermediate oxidation state.

Results of the analysis of Mo K-edge EXAFS data for all of the $n[MoO_{3-x}]-Na_{56}Y$ materials are included in Table I. Unlike the various tungsten oxide materials reported elsewhere,[2,4–8] in which dimers were detected by the presence of a W–W "second shell" scattering contribution, the molybdenum EXAFS gave no evidence of this. Even when k^3 weighting was used as a means of emphasizing any such features, a Mo–Mo shell was observed for neither the $n[MoO_3]-Na_{56}Y$ nor the $n[MoO_2]-Na_{56}Y$ samples. Structural models consistent with the EXAFS results for $n[MoO_3]-Na_{56}Y$ and $n[MoO_2]-Na_{56}Y$ comprise MoO_{3-x} moieties anchored by three O atoms in a zeolite six-ring site (or conceivably the two O atoms of a four-ring site). These are clearly related to various $LMoO_3$ complexes[18] (where L = 1,4,7-triazacyclononane or N,N',N''-trimethyl-1,4,7-triazacyclononane) which are, interestingly, formed by the oxidative decarbonylation of $LMo(CO)_3$ precursors.

The application of ^{23}Na MAS/DOR-NMR has provided insight about "secondary" anchoring interactions between the MoO_3 and MoO_2 moieties and the α-cage Na^+ cations.[15] As in the case of the various encapsulated WO_{3-x} moieties, there was evidence for site II Na^+ cation adsorption-induced chemical shifts and intensity alterations for both $n[MoO_3]-Na_{56}Y$ and $n[MoO_2]-Na_{56}Y$. Each of these zeolite Y encapsulated monomers tends to participate in secondary anchoring interactions which involve the oxygen end of at least one of their terminal oxometal groups and a site II Na^+ cation.

(18) Roy, P. S.; Wieghardt, K. *Inorg. Chem.* 1987, *26*, 1885.

Smart Zeolites

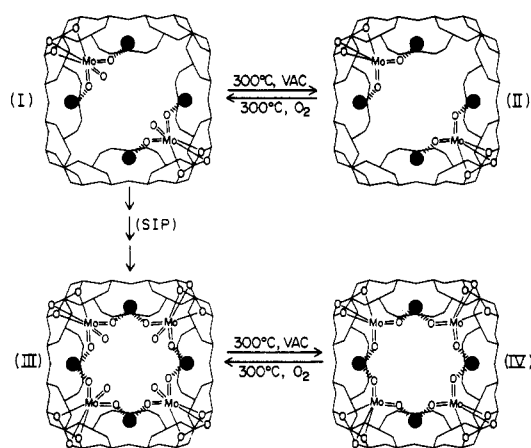*Acc. Chem. Res., Vol. 25, No. 12, 1992* **559**

Figure 5. Structures of the various zeolite-encapsulated molybdenum oxides and their thermal vacuum reduction products.

All of these structural proposals for the molybdenum system are conveniently summarized in Figure 5 and are presented along with the comparable structures for the tungsten system, Figure 2, in order to highlight the similarities and differences between the two systems.

Electronic and Optical Properties. A recent quantitative kinetic study[19] of the substitution reactions of ^{12}CO in $n[Mo(CO)_6]-M'_{56}Y$ (where $M' = $ Li, Na, K, Rb, Cs; $0 < n \leq 16$) by ^{13}CO and $P(CH_3)_3$ has confirmed the existence and importance of ZOM···OC interactions. The activation parameters varied systematically with the number, ionic potential, and spatial demands of the α-cage site II and III cations and were shown to be substantially different from those of the corresponding gas- and liquid-phase reactions. The implied modification of the electronic environment of the molybdenum center (and hence its ligands) by the zeolite host is clearly relevant to the potential use of zeolite-encapsulated molybdenum oxides as catalytic materials.

$Mo(3d_{5/2})$ core level binding energies were measured by XPS (to within ± 0.4 eV), for the $n[Mo(CO)_6]-Na_{56}Y$ precursor samples as well as the various oxide products. The binding energy value of 227.8 eV for $16[Mo(CO)_6]-Na_{56}Y$ is shifted upward by 1.6 eV relative to that[20] of bulk $Mo(CO)_6$. This implies some degree of charge transfer from the $Mo(CO)_6$ guest to the $Na_{56}Y$ host, which can be attributed to cation anchoring of the type described earlier, rather than to a formal oxidation process. A 5.8-eV upward shift of the $Mo(3d_{5/2})$ binding energy for $16[MoO_3]-Na_{56}Y$ relative to that of the zerovalent precursor is consistent with the photooxidation product being zeolite Y encapsulated molybdenum(VI) oxide (a shift of approximately 1 eV in the $Mo(3d_{5/2})$ binding energy corresponds[3] to a change of one formal oxidation state). Similarly, the observation that the $Mo(3d_{5/2})$ binding energy in $16[MoO_2]-Na_{56}Y$ was 1.9 eV lower than that in $n[MoO_3]-Na_{56}Y$ is strongly supportive of the notion that thermal reduction involves a two-electron-reduction process between oxomolyb-

denum(VI) and oxomolybdenum(IV) centers. The XPS probe also yields information about the mechanism of photooxidation of $n[Mo(CO)_6]-Na_{56}Y$ to $n[MoO_3]-Na_{56}Y$. In situ MID-IR monitoring of the reaction indicated no observed CO, implying an oxidation process wherein either ligated or gaseous CO groups were transformed to CO_2, by either gaseous O_2, coordinated O_2, or oxometal groups. Complementary to this, XPS gave no evidence of carbonaceous deposition which might have resulted from, for example, the Boudart disproportionation reaction:[21] $2CO \rightarrow CO_2 + C$ (which itself might have been catalyzed or photocatalyzed by the zeolite, molybdenum carbonyl, oxide, or any metallic reaction intermediate).

On the basis of the structural model (discussed earlier) for $16[MoO_3]-Na_{56}Y$, the broad, intense UV absorption band centered around 280 nm has been assigned to $O^{2-}(2p\pi) \rightarrow Mo^{6+}(4d)$ LMCT excitations. This assignment is consistent with those proposed[22] for Mo^{6+} complexes having comparable coordination environments. The LMCT region shows a tendency to broaden and red shift (as did the corresponding feature for the W^{6+} moieties) with increasing loading over the range $0 < n \leq 16$. This most likely results from through-bond and/or through-space intracavity and/or intercavity coupling between the *fac*-trioxomolybdenum(VI) moieties. In the case of $16[MoO_2]-Na_{56}Y$, the intense broad UV absorption band centered near 240 nm is assigned to $O^{2-}(2p\pi) \rightarrow Mo^{4+}(4d)$ LMCT excitations. It also demonstrates a tendency to broaden and red shift with increasing loading over the range $0 < n \leq 16$, likewise indicating intra/intercavity coupling between *cis*-dioxomolybdenum(IV) units. The intense visible absorptions (responsible for the puce color of $n[MoO_2]-Na_{56}Y$) centered around 460 and 510 nm are best assigned to 4d–4d ligand field transitions, which are consistent with those proposed for other comparable Mo^{4+}, d^2 complexes.[23]

As discussed earlier, ^{23}Na MAS- and DOR-NMR spectra clearly indicate site II Na^+ cation interactions[3,15] in both products $n[MoO_{3-x}]-Na_{56}Y$ ($x = 0$, 1). This strongly suggests that the oxygen atom of at least one of the terminal oxometal groups in the monomeric *fac*-trioxomolybdenum(VI) moiety and both oxometal groups in the *cis*-dioxomolybdenum(IV) moiety may bind to site II Na^+ cation(s). A comparison exists between such binding in these moieties, and the ligating properties of the MoO_3 moiety in $LMoO_3$ complexes toward cationic metal centers.[18] For example, reaction of $LMoO_3$ with $Co(ClO_4)_2\cdot 6H_2O$ in dry methanol yields a blue solution from which crystals of the composition $[(LMoO_3)_4Co](ClO_4)_2$ precipitate, whereas the same reaction carried in aqueous solution produces a pink solution containing $[Co(H_2O)_6]^{2+}$. This indicates that the oxygen atoms of the $LMoO_3$ units are weaker donor ligands than water but stronger than methanol.[18] This, along with the other examples discussed above, clearly illustrates how the zeolite cavity acts as a macrospheroidal multidentate ligand ("zeolate") toward various guests.[19]

(19) Ozin, G. A.; Özkar, S.; Pastore, H. O.; Poë, A. J.; Vichi, E. J. S. *J. Chem. Soc., Chem. Commun.* **1991**, *141*. Ozin, G. A.; Özkar, S.; Pastore, H. O.; Poë, A. J. In *Supramolecular Architecture in Two and Three Dimensions*; ACS Symposium Series 499; American Chemical Society: Washington, DC, 1992; p 314; Intrazeolite Metal Carbonyl Kinetics: Substitution Reactions of $Mo(^{12}CO)_6$ in Zeolite Y. *J. Am. Chem. Soc.*, in press. Ozin, G. A.; Özkar, S. Zeolates: A Coordination Chemistry View of Metal–Ligand Bonding in Zeolite Guest–Host Inclusion Compounds. *Chem. Mater.* **1992**, *4*, 511.

(20) Lichtenberger, D. L.; Kellog, G. E.; Landis, G. H. *J. Chem. Phys.* **1985**, *83*, 2759.

(21) Ichikawa, S.; Poppa, H.; Boudart, M. *J. Catal.* **1985**, *91*, 1.

(22) Iwasawa, Y.; Sato, Y.; Kuroda, H. *J. Catal.* **1983**, *82*, 289.

(23) Lever, A. B. P. *Inorganic Electronic Spectroscopy*, 2nd ed.; Elsevier Publ.: Amsterdam, 1984.

Conclusions

A clean, mild, and quantitative series of impregnations of the $M(CO)_6$ precursor, followed by photooxidation in the presence of O_2 and/or vacuum thermal reductions and/or reversible reoxidation, has yielded new forms of tungsten and molybdenum oxides $n[MO_{3-x}]-M'_{56}Y$ (where $0 < n \leq 32$; M = Mo or W; x = 0, 1 for Mo and x = 0, $^1/_2$, 1 for W; and M' = H, Li, Na, K, Rb, Cs). In all such materials, the Mo- and W-containing moieties are strictly confined within the internal void space (exclusively α-cage) of the zeolite host. Each of the impregnation, oxidation, and reduction steps has been shown to result in perturbation of neither the host lattice crystallinity nor its integrity, and in only very slight changes in the unit cell size.

Structural characterization techniques applied to these materials have revealed that well-defined monomeric, dimeric, and tetrameric molecular tungsten oxides $n[WO_{3-x}]-Na_{56}Y$ exist exclusively in the α-cages of the $Na_{56}Y$ zeolite host. For x = 0 materials ($n \geq 16$), only dimers were observed; for the x = $^1/_2$ samples, dimers resulted at half-loading (n = 16) but a tetrameric structure resulted at n = 32; and for x = 1, only framework-oxygen-anchored monomers were produced at any loading. The $Rb_{56}Y$ analogs demonstrated comparable structural behavior for materials in which x = $^1/_2$ or 1, but in contrast, the $16[WO_3]-Rb_{56}Y$ materials were oxygen framework anchored and monomeric rather than dimeric. This difference was attributed to the steric limitations posed by having six larger Rb^+ cations rather than four smaller Na^+ in each α-cage, and the inflexibility of the $W(\mu-O)_2W$ bridging group in the W_2O_6 dimer. The molybdenum oxides $n[MoO_{3-x}]-Na_{56}Y$ (where $0 < n \leq 32$ and x = 0, 1) were also shown to be well defined and uniform, although only framework-oxygen-anchored monomers were generated in any of the systems examined.

Measurements made by XPS spectroscopy have clearly demonstrated that the oxidation states +6, +5, and +4 (representing x = 0, x = $^1/_2$ and x = 1, respectively) can be assigned to the tungsten centers in $n[WO_{3-x}]-Na_{56}Y$. Similarly, for the molybdenum oxide materials $n[MoO_{3-x}]-Na_{56}Y$, the products contained +6 and +4 moieties. In the special case of the W_2O_5 dimer, XPS results indicated that both tungsten centers were in the +5 oxidation state rather than members of a mixed-valence +4/+6 moiety. Band assignments in the UV–visible spectra were also consistent with this conclusion.

Depending on the degree of filling of the α-cage void volume by these MO_{3-x} units, one can visualize them as either *isolated* or *coupled* (through space and/or the zeolite framework) within a molecular orbital or miniband type description[17] of their electronic properties. Such is manifested in the observed loading dependent red shifts in the UV and visible spectra, and demonstrates that it is possible to have precise control of the oxidation state, degree of n-doping, and extent of miniband filling[17] of a metal oxide supralattice composed of organized assemblies of single size and shape molecular metal oxides. Thus, the ability to fine tune the structural and electronic properties of $n[MO_{3-x}]-M'_{56}Y$ materials can be considered to make them rather "smart" zeolites and may prove valuable in the areas of catalysis, solid-state chemistry, and materials science.

Registry No. WO_3, 1314-35-8; MoO_3, 1313-27-5.